Surface & Coatings Technology 479 (2024) 130538

Contents lists available at ScienceDirect

Surface & Coatings Technology

journal homepage: www.elsevier.com/locate/surfcoat

Effect of surface pretreatment on the production of LDH for post-treatment with benzoxazine resin

Roya Malekkhouyan [a], Louis Van Renterghem [b], Leila Bonnaud [d], Yoan Paint [d], Maurice Gonon [a], David Cornil [c], Jérôme Cornil [c], Jean-Marie Raquez [b], Marie-Georges Olivier [a,d,*]

[a] Materials Science Department, Mateirlas Institute, University of Mons, Place du parc 20, Mons 7000, Belgium
[b] Laboratory of Polymeric and Composite Materials (LPCM), Center of Innovation and Research in Materials, University of Mons (UMONS), Place du Parc 20, Mons 7000, Belgium
[c] Laboratory for Chemistry of Novel Materials, University of Mons (UMONS), 20 Place du Parc, Mons B-7000, Belgium
[d] Materia Nova Research Center, Parc Initialis, 7000 Mons, Belgium

ARTICLE INFO

Keywords:
Magnesium
Corrosion
Plasma electrolytic oxidation
Conversion coating
Layered double hydroxide
Benzoxazine resin

ABSTRACT

In the present study, the surface of AZ31 Mg alloy was pretreated by etching in nitric acid and plasma electrolytic oxidation (PEO). Then Mg-Al layered double hydroxide (Mg-Al/LDH) was synthesized on the pretreated surface of substrates via hydrothermal treatment to increase the corrosion resistance. The effect of surface pretreatment (etched substrate and PEO layer) on LDH formation, structure, and corrosion resistance was investigated. Benzoxazine resin (thermosets), has been used for coatings, however, the high curing temperature limits their applications. For this purpose, a new bio-based benzoxazine resin with a lower curing temperature (160 °C) was developed to be applicable for Mg alloys. Phenol (Phloretic acid), diol (Dodecandiol), and amine (monoethanolamine) were used to synthesize innovative benzoxazine with exchangeable ester functions and self-healing ability. This resin was further used for post-treatment of LDH samples. The morphology, chemical composition, and crystalline structure of LDH samples were characterized by scanning electron microscopy (SEM), energy-dispersive X-ray spectroscopy (EDS), and X-ray diffraction (XRD). The corrosion resistance of the coatings was investigated by salt spray test as well as electrochemical impedance spectroscopy (EIS). The LDH layer on the etched substrates showed better corrosion resistance than the LDH on PEO layer due to having a thicker inner layer (11.8 ± 0.2 μm and 7.0 ± 0.6 μm for LDH on the etched substrate and PEO layer, respectively). Post-treatment of samples with benzoxazine resin showed the effective capability of this polymeric coating for enhancing the corrosion resistance of Mg alloy substrate. This benzoxazine coating increased the corrosion resistance of the coating/substrate system around 10^4 times in comparison to the bare substrate. Moreover, it was observed that the LDH layer can increase the adhesion and compatibility of the substrate with benzoxazine resin. These results were confirmed by EIS and cross-cut adhesion tests experimentally as well as theoretical calculations of the adsorption energy of benzoxazine molecule to the LDH layer using Density Functional Theory (DFT).

1. Introduction

Recently, magnesium alloy substrates have attracted attention due to desirable properties (like high strength-to-weight ratio), making them suitable for different applications including transportation, aerospace, and electronic parts [1]. However, they suffer from low corrosion resistance due to their intrinsic active nature [2]. In this regard, plasma electrolytic oxidation (PEO) can be used to increase the corrosion resistance of the substrates as an efficient surface pretreatment [3]. During the PEO process, a voltage (more than the breakdown voltage) is applied to the substrate and an anodic layer is produced as the result of the oxidation reaction. Applied potential acts as the driving force for the formation of the oxide layer [1]. The formed layer is porous due to the evolution and entrapment of oxygen gas as well as electrolyte vapors [4], and thermal stresses formed during the fast solidification of the produced molten oxide [1,5]. For these reasons, this porous layer should be further sealed. The composition of PEO coating as well as its structure can be changed concerning the electrolyte chemicals. The addition of

---

* Corresponding author at: Materials Science Department, Mateirlas Institute, University of Mons, Place du parc 20, Mons 7000, Belgium.
E-mail address: marjorie.olivier@umons.ac.be (M.-G. Olivier).

https://doi.org/10.1016/j.surfcoat.2024.130538
Received 12 January 2024; Received in revised form 6 February 2024; Accepted 8 February 2024

aluminate and phosphate can increase the wear and corrosion resistances, thickness, and roughness of PEO coatings [6,7]. Moreover, KOH affects the properties by changing the conductivity of the electrolyte (increasing KOH concentration increases the conductivity) [8]. However, further increases in electrical conductivity can cause the production of large pores [9].

Layered double hydroxide (LDH) as a surface pretreatment is composed of di- and trivalent metal cations in the layered structure with a combination of anions in the interlayer [10]. LDH can enhance the corrosion resistance of substrates by their anion-exchange property as well as entrapping corrosive ions in electrolytes like Cl^-. Moreover, LDH can be formed on the PEO layer for sealing the existing pores. In this case, the dissolution of the PEO layer can be the source of metal cations. For instance, the electrolytes containing aluminate can eliminate the need for further addition of Al salts [11]. The formation of Mg-Al/LDH on the PEO layer containing MgO and Al_2O_3 highly depends on the hydrolysis of these two compounds on the solid particles of the PEO layer [12].

Organic coatings are another cost-effective method used in industry for the protection of Mg alloys [13] and due to the corrosion mechanism of Mg, alkaline-resistance resin should be used [14]. As a barrier layer, organic coatings have the ability to prevent Mg alloys from corrosion. However, their adhesion to the substrate must be enhanced by appropriate surface pretreatment. The adhesion is an important factor as Grundmeier et al. [15] showed corrosion is more dependent on adhesion than the diffusion of corrosive ions to the substrate. According to the literature resins like polyvinyl butyral, vinyl epoxy, acrylic, polyurethane, or baked phenolic can be applied for corrosion protection of Mg alloys [14]. Recently, benzoxazine resins have attracted attention due to their proper thermal and mechanical properties, high chemical resistance, appropriate glass transition temperature, and low shrinkage after curing [16,17]. Moreover, their usage as the organic coating for the protection of Al alloy substrates has shown good corrosion protection [18].

The first benzoxazine monomers were synthesized by the condensation reaction of amine, formaldehyde, and phenol [19]. The benzoxazine ring which consists of an oxazine ring attached to the benzene ring (with phenol, diol, and amine precursors) can be opened by thermal activation and cathodic polymerization [20]. By varying phenolic and amine precursors different benzoxazine monomers upon the desired properties can be obtained. For example, the high curing temperature, hard to process, and brittleness can be controlled by changing the precursors [17]. Polybenzoxazines exhibit alkaline resistance, and their adhesive properties make them suitable as primers [21].

The combination of surface pretreatments along with organic coating can be an approach for increasing the corrosion resistance of substrates. In most of the studies related to organic coating with LDH, only a biocompatible organic coating was used for potential biomedical applications [22]. In this study, the effect of surface pretreatment on the formation of LDH and the corrosion resistance of AZ31 Mg alloy was investigated. Moreover, a new type of benzoxazine resin with lower curing temperature and self-healing ability (due to transesterification) was applied on the LDH surface to assess the compatibility of the organic and inorganic coatings. According to the results, LDH on the etched substrate can successfully protect the substrate better than LDH on PEO layer. Moreover, benzoxazine resin improved the corrosion resistance of the substrates. In addition, the related compatibility of LDH layer with benzoxazine resin was highlighted using adhesion test and DFT calculations.

2. Experimental section

2.1. Materials

AZ31 Mg alloy with a composition of 2.5–3.5 % Al, 0.7–1.3 % Zn, 0.2 % Mn, 0.05 % Si, 0.05 % Cu, 0.04 % Ca, 0.005 % Fe, 0.1 % Ni (wt%) and balance Mg (supplied from KG Fridman AB (SWEDEN)) was used for the substrate. NH_4NO_3, and $Al(NO_3)_3.9H_2O$ were purchased from RPL, and EMPLURA, respectively. $Al_2O_3Na_2O$ was obtained from Alfa Aesar, and KOH was supplied from Honeywell. Phloretic Acid (>98 %) was purchased from TCI and NaOH, $Na_6O_{18}P_6$, 1,12-Dodecandiol (99 %), Methyl Ethyl Ketone, Dioxolane, and paraformaldehyde were obtained from VWR chemicals.

2.2. Surface pretreatment

Etching and PEO were used as surface pretreatments for the AZ31 Mg alloy. For this purpose, etching was performed by immersing samples in 0.25 M and 2 M HNO_3 solution for 60 s and 30 s, respectively. The anodic layer was produced on the etched surface of samples in an electrolyte containing 7 g/L KOH, 4 g/L $Al_2O_3Na_2O$, and 7 g/L $Na_6O_{18}P_6$ (due to the appropriate wear and corrosion resistance properties of aluminate and phosphate based electrolyte [6]) with pH = 12 and the conductivity of 26 mS/cm (at room temperature) which was measured by conductivity meter (CO 3100L VWR).

The PEO coating was produced for 360 s using a pulsed AC power supply with a square electrical signal (+400 V/−30 V). The frequency and duty ratio were 67 Hz and 33 %, respectively. The thickness of the produced PEO layer was measured to be 4.7 ± 0.5 μm (using cross-section SEM images).

2.3. LDH formation on the pretreated surfaces

LDH was formed on the surface of the etched substrate and PEO layer. The LDH preparing solution contained 0.6 M NH_4NO_3 and 0.1 M $Al(NO_3)_3$ (to provide Al element for participating in LDH structure on bare substrate [23]). The pH of the solution was increased to 11 by the addition of 2 M NaOH solution. The pretreated surfaces (etched and PEO) were placed in a Teflon-lined autoclave along with the prepared solution. The autoclaves were then heated to 125 °C for 24 h. The samples with LDH on etched and PEO surfaces are coded as ELDH and PLDH, respectively.

2.4. Organic coating preparation

2.4.1. Ester synthesis

PA-dodecandiol was prepared using 120 mmol of Phloretic acid reacted, 72 mmol of Dodecandiol, and 1 mmol of paratoluenesulfonic acid. All the reagents were placed into a 250 mL beaker equipped with a stirring bar. The mixture was stirred at 130 °C for 24 h at 150 rpm. After cooling to room temperature, the crude product was solubilized in 200 mL of Methyl Ethyl Ketone. Then, the solution was washed with deionized water three times to remove the catalyst. The organic solvent was dried under vacuum overnight to obtain a dark red viscous product yield of 92–95 %. ^1H NMR (DMSO-d_6,ppm): 9.18 (Ar-OH*), 6.97 (Ar*-OH), 6.67 (Ar*-OH), 3.98 (O=C-O-CH2*), 2.75 (HO-AR-CH2*), 2.55 (HO-AR-CH2-CH2*), 1.53 (O=C-O-CH2-CH2*), 1.25 (DD-CH2*-CH2*-).

2.4.2. Benzoxazine synthesis

The synthesis of PA-dodecandiol-mea was performed according to the following way. 60 mmol of Phloretic ester reacted with 120 mmol of monoethanolamine and 240 mmol of paraformaldehyde into a 250 mL beaker equipped with a stirring bar. The mixture was stirred at 85 °C for 150 min and 30 min at 90 °C at 150 rpm. The resulting product was a dark red viscous liquid. ^1H NMR (DMSO-d_6,ppm): 6.92–6.63 (Ar*-oxazine), 4.79 (N-CH2*-O-Ar), 4.51, 3.98 (O=C-O-CH2*), 3.93 (N-CH2*-Ar), 3.56 (HO-CH2*-CH2), 2.72 (AR-CH2* + HO-CH2-CH2*), 2.55 (AR-CH2-CH2*), 1.51 (O=C-O-CH2-CH2*), 1.23 (DD-CH2*-CH2*-). FTIR (cm^{-1}): PA-dodecandiol-mea: 1700 (C=O stretching from the ester), 1230 (C-O-C stretching asymmetric), 1118 (C-H inplane bending mode 18a and 18b), 1034 (C-O-C stretching symmetric), 937 (C-H out of plane bending vibration bands oxazine mode 10a and trisubstituted benzene).

2.5. Coating pretreated substrates

The samples with dimensions of 5 × 4 cm^2 were coated by benzoxazine resin using solvent casting. For this purpose, 0.05 g of monomer was dissolved in 1 mL of acetone, and using a pipet the prepared solution was homogenously applied on the samples. The coated samples were kept at room temperature (23 ± 0.5 °C) for 2 h to remove the solvent (evaporation of acetone), and then they were heated up to 160 °C for 2 h to cure the benzoxazine. The thickness of the obtained benzoxazine coatings on Mg, PEO, ELDH, and PLDH was 13 ± 4, 14 ± 4, 12 ± 1 μm, and 12 ± 2 μm, respectively.

2.6. Characterization

The surface morphologies, and thickness of layers, as well as the elemental composition of PEO and LDH layers, were investigated by scanning electron microscope (SEM, Hitachi SU8020) equipped with an energy dispersive X-ray spectrometer analyzer (EDS, Thermo Scientific Noran System 7). To obtain cross-section images, samples were embedded in resin (EpoFix resin and EpoFix hardener) and Struer TegraForce-5 was used for grounding them with 800, 1200, 2000, and 4000 SiC papers. The crystalline structure of surfaces was investigated with X-ray diffraction (XRD, Panalytical Empyrean Theta – Theta) with CuKα radiation (λ = 0.154056 nm) and Ni filter with a step of 0.02° and a scanning rate of 1.2°/min in the 2θ range from 4° to 70°. Moreover, the adhesion test was performed according to ISO 2409. The surface roughness of the samples was measured utilizing the digital microscope HIROX KH-8700.

The electrochemical impedance spectroscopy (EIS) was performed in 0.1 M NaCl solution, saturated with $Mg(OH)_2$ using a ModulLab controlled by XM-Studio® software. A classical three-electrode system, which consisted of a platinum counter electrode, an Ag/AgCl (sat. KCl) reference electrode, and samples, as working electrodes with an exposed area of 0.78 cm^2 were used. EIS measurements were performed in a frequency range from 100 kHz to 100 mHz with 61 points using a 10 mV peak-to-peak sinusoidal voltage. These conditions were used for EIS measurements of samples without organic coating, however, for the samples with organic coating, the exposed area was 7.06 cm^2 in 0.1 M NaCl solution and a 30 mV peak-to-peak sinusoidal voltage was applied. The salt spray test was carried out using Q-LAB Model SSP equipment according to the ASTM B117 on intact samples with and without organic coating. The thickness of organic coatings was measured using Elcometer® 456. Each experiment was performed at least three times.

2.7. Density functional theory (DFT)

Quantum-chemical calculations were carried out to better understand the chemical interactions between the organic coating and Mg-based substrates. A simplified version of the organic coating (Fig. 1), generated by keeping one part of the symmetric experimental molecular compound, was used to facilitate the computations. The impact of the substrate's composition on the organic coating adhesion was investigated by comparing the interaction energy of the organic molecule with 4 surfaces: a) pristine magnesium (Mg), b) magnesium oxide (MgO), c) magnesium hydroxide ($Mg(OH)_2$), and d) Mg:Al hydroxide with carbonate between the layers ($Mg_6Al_2(CO_3)(OH)_{16}$) for Mg-Al/LDH. These calculations were done at the Density Functional Theory (DFT) level with a periodical slab approach using the Vienna Ab Initio Simulation Package (VASP) [24,25]. The projected augmented wave (PAW) scheme with a plane-wave basis set of 500 eV was used. The exchange-correlation was treated using the PBE functional [26] and Van der Waals interactions described with the DFT-D3 grimme approach [27,28].

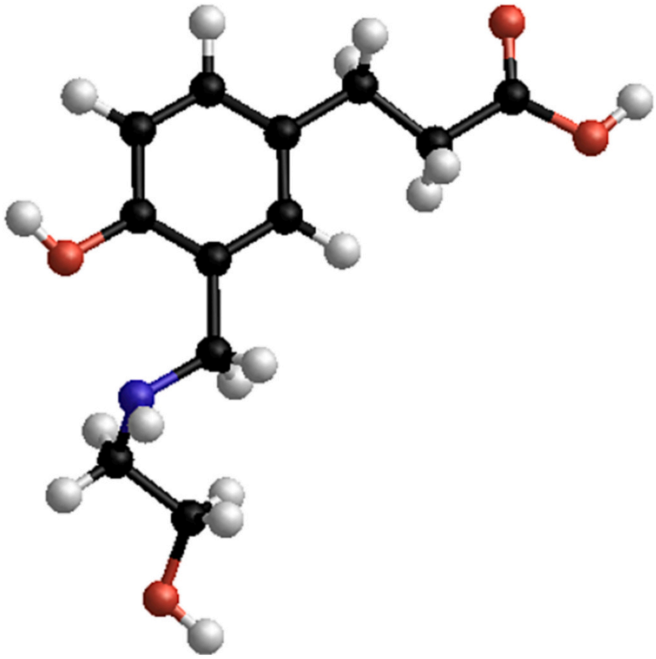

Fig. 1. Simplified model of benzoxazine molecule for DFT calculations (the black, white, red, and blue balls stand for C, H, O, and N atoms, respectively). (For interpretation of the references to colour in this figure legend, the reader is referred to the web version of this article.)

3. Results and discussion

3.1. Morphological and chemical characterizations

Fig. 2 shows the SEM images of the surface and cross-section for the samples. Fig. 2(a) shows the layered structure of LDH on the surface. The SEM image of PEO surface shows typical pores related to the oxygen and hydrogen gas evolution as well as electrolyte vapors [1,4]. Moreover, from Fig. 2(c), it can be observed that the small pores in the structure of PEO layer (Fig. 2(b)) are filled with LDH and they are formed inside of the bigger pores (Fig. 2(c)). Fig. 2(d-f) display the cross-section of samples. After the formation of LDH, two layers have been created, the inner compact layer and the porous outer layer in both LDH samples (on the etched substrate and PEO layer). These layers are shown in Fig. 2(d-f). In the case of sample PLDH, after the formation of LDH an inner compact layer is formed with a decrease in the PEO layer thickness (the thickness of PEO layer in Fig. 2(e) is 4.7 ± 0.5 μm and after LDH formation in Fig. 2(f) it decreases to 3.3 ± 0.6 μm) indicating the inability of complete dissolution of PEO layer. This compact inner layer is due to the inward growth of the coating [29,30]. The thickness of the inner layer for ELDH and PLDH are 11.8 ± 0.2 μm and 7.0 ± 0.6 μm, respectively, which is lower for PLDH due to the existence of the PEO layer and limitations for dissolving.

EDS results from the cross-section of samples can be seen in Fig. 3. The EDS cross-sections for LDH samples in Fig. 3(a), (c) show Al element concentrated on the surface which is attributed to the LDH formation [31]. Moreover, the elemental composition of the PEO layer (O, Mg, Al, and P) in Fig. 3(b), (c) can be observed. According to EDS results and literature, the inner layer is mainly composed of $Mg(OH)_2$ [29].

The XRD diagrams of samples are presented in Fig. 4. The characteristic peaks of Mg, $Mg(OH)_2$, and LDH are marked in this figure according to JCPDS No. 00-035-0821, 00-007-0239, and 00-038-0478, respectively. The characteristic peaks at 43.35° can be attributed to the MgO in the PEO layer for PEO and PLDH samples [29]. In the samples with LDH, $Mg(OH)_2$ peaks at 18.43° and 38.02° show the dissolution of Mg for the production of LDH [32]. The LDH characteristic peaks in both

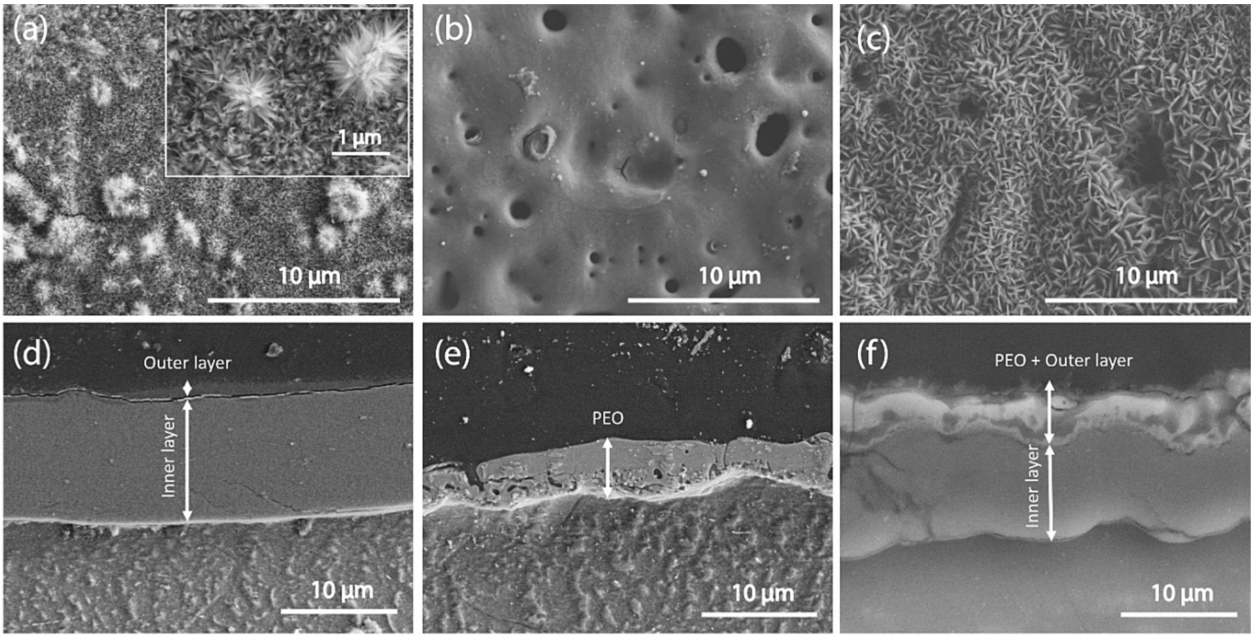

Fig. 2. SEM images of surface: a) ELDH, b) PEO, c) PLDH, and cross-section: d) ELDH, e) PEO, f) PLDH.

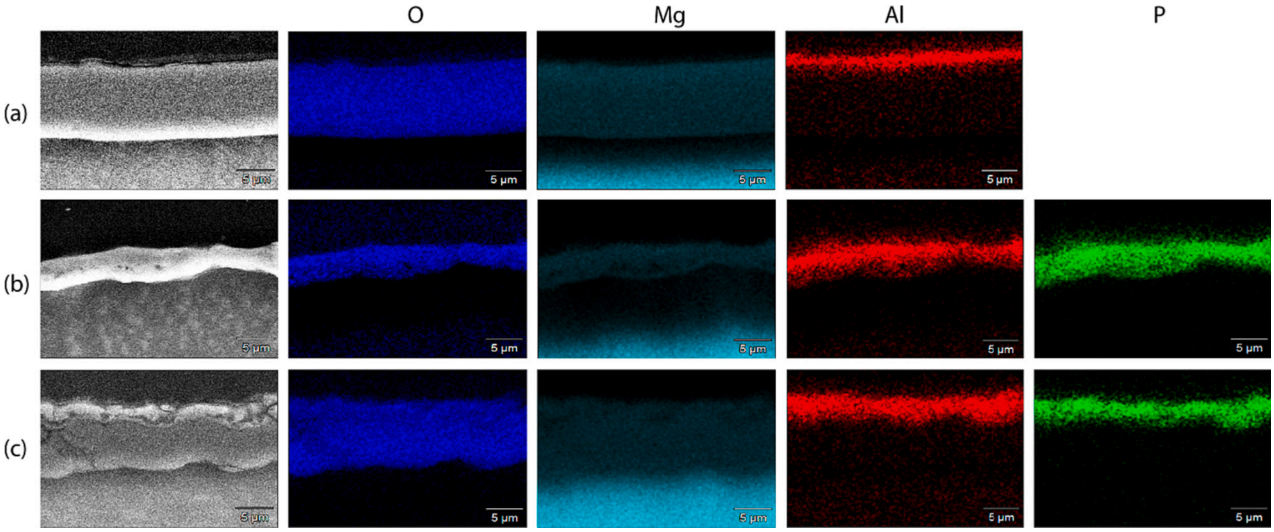

Fig. 3. EDS mapping of the cross-section of a) ELDH, b) PEO, and c) PLDH.

of the samples with LDH are also observed at 11.5° and 23.3° related to (003) and (006), respectively [12]. According to the literature, the concentration of Mg can affect the layer charge density and change the configuration of the intercalated anion [33]. In the case of LDH formation on the bare substrate, the dissolved Mg (Mg^{2+} cations) and consequently $Mg(OH)_2$ is more than LDH on the PEO layer according to SEM images of cross-section and XRD diagram (higher-intensity $Mg(OH)_2$ peaks for ELDH), which leads to a smaller sized (lateral) LDH (Fig. 2). Important peaks are highlighted in Fig. 4.

3.2. *Electrochemical measurements (EIS)*

The graphical representations related to the EIS results of immersed samples in 0.1 M NaCl solution are indicated in Fig. 5.

At the frequency of 0.1 Hz, the value of impedance, denoted as $|Z|$, shows the overall substrate/coating's impedance. This value is indicative of the protective quality of the coating against corrosion [31]. Comparing these values for samples shows the highest amount for PEO and ELDH ($>10^5$ Ω.cm^2) after 1 h immersion. With passing time to 7 days, the impedance modulus at low frequency decreased for PEO to $<10^4$ Ω.cm^2 while for the samples with LDH, this amount is $>10^4$ Ω.cm^2. For the bare substrate (denoted as Mg in the figure), the impedance modulus at frequency of 0.1 Hz was decreased after 24 h immersion (from 1892 Ω.cm^2 to 1170 Ω.cm^2), then it was increased after 7 days (2266 Ω.cm^2) that can be related to the formation of corrosion products on the surface [31].

The phase angle at high frequency, indicative of the protective capability of the outer layer, reaches its maximal absolute value for ELDH after 1 h of immersion in the NaCl solution, at approximately −50°. The decrease in the absolute value of phase angle to below −30° at high frequency after 7 days of immersion for all the samples indicates the loss of protection [31]. Moreover, the most decrease was related to the PEO sample (after bare substrate). After 1 day of immersion, all samples displayed an inductive loop, which can be attributed to the non-

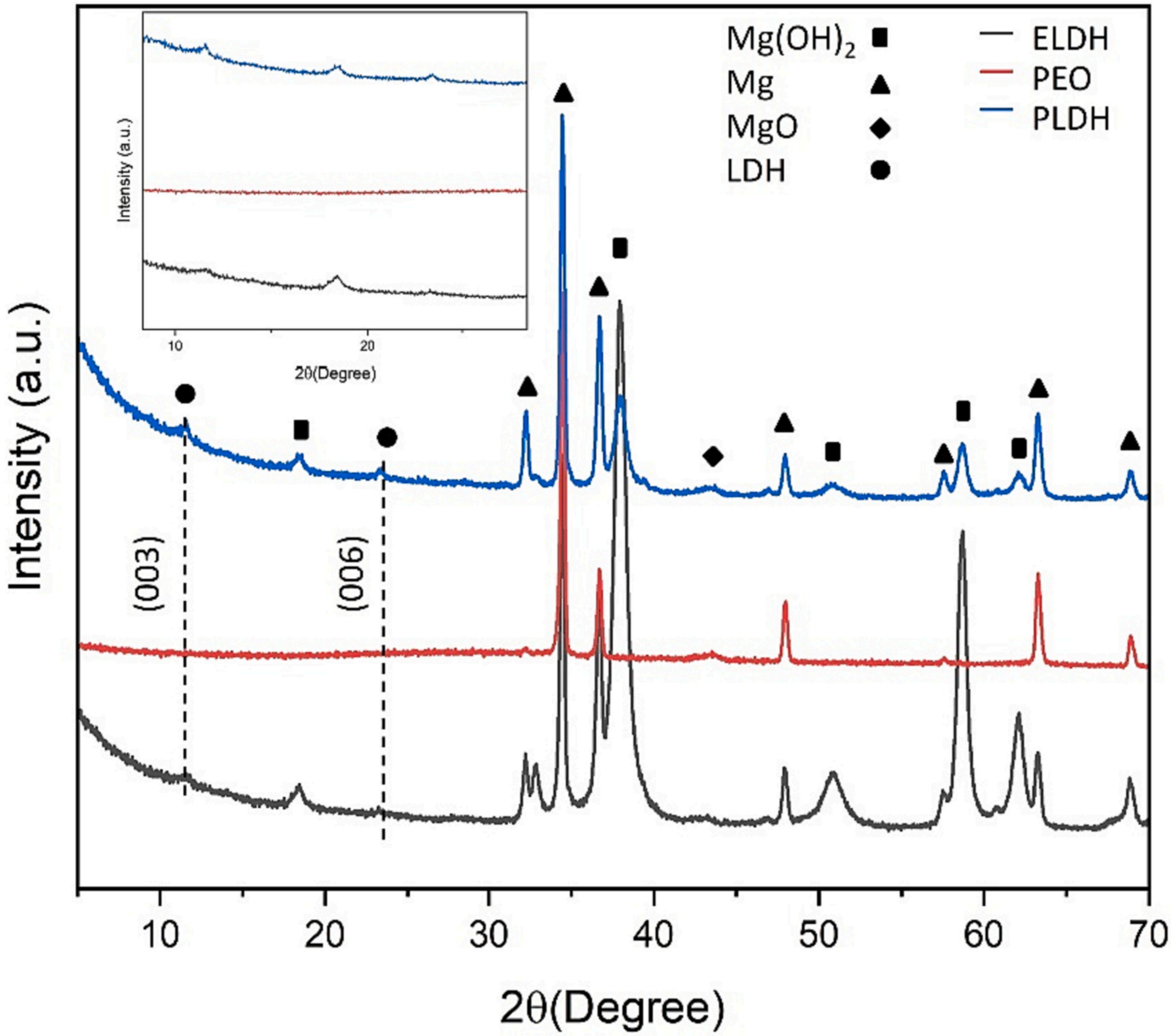

Fig. 4. XRD diagrams of a) ELDH, b) PEO, and c) PLDH.

stationarity of the Mg alloy substrates and EIS measurements [34].

EIS is also used to assess the evolution of the corrosion activity of the coating in 0.1 M NaCl solution. After being immersed for 7 days, LDH coatings maintained their impedance modulus at 0.1 Hz (~10^4 Ω.cm^2) indicating proper corrosion resistance of these samples. At intermediate frequency (from 10^0 to 10^2 Hz), the phase angle of PEO coating decreases more than two other samples after 7 days of immersion, representing the penetration of the electrolyte into the coating system and the beginning of electrochemical reactions under the coating.

The electrochemical properties and specific structural characteristics of the coatings are analyzed using equivalent circuit models [31]. Fig. 6 (a) shows equivalent circuits used for analyzing and fitting EIS results for samples after 1 h immersion and Fig. 6(b) for 1 day and 7 days immersion. For PEO after 1 h of immersion circuit in Fig. 6(c) and for bare substrate during all immersion times, Fig. 6(d) were applied. In these circuits, the resistance and constant phase elements of the outer porous layer and compact inner layer of coatings are presented by out and in, respectively. Microcracks or micropores in the coating allow corrosive species to invade the metal interface, which will cause the Mg matrix to corrode. The interface of substrate-electrolyte response capacitance is represented by CPE$_{dl}$ and the charge transfer resistance is interpreted as R$_{ct}$ throughout the corrosion evolution. The value of impedance at low frequency (0.1 Hz) and R$_{ct}$ (in Table 1 and Fig. 7(a), (b)) changed with passing time, showing decrease of the barrier properties of the coating and increasing corrosion rate (due to decreasing R$_{ct}$) [35]. However, comparing R$_{ct}$ shows higher values for samples with LDH representing lower corrosion rates that can be attributed to the thick inner layer of LDH and better protectivity of these coatings. In addition, R$_{out}$ and R$_{in}$ of all coatings reflecting resistance of outer and inner layers, have a downward trend after 7 days immersion, indicating reduction of the corrosion resistance. The comparison of these results with the results of LDH with corrosion inhibitors in the literature [12], shows better protectivity of the LDH coatings in this study. In the equivalent circuits, the capacitance of the outer and inner layers are shown with CPE$_{out}$ and CPE$_{in}$, respectively. Fig. 7(c) shows the values of CPE$_{in}$ are at the lowest position for samples with LDH especially for ELDH (higher inner layer thickness for ELDH) representing the compact inner layer and better corrosion resistance. The results of fitting EIS data are presented in Table 1.

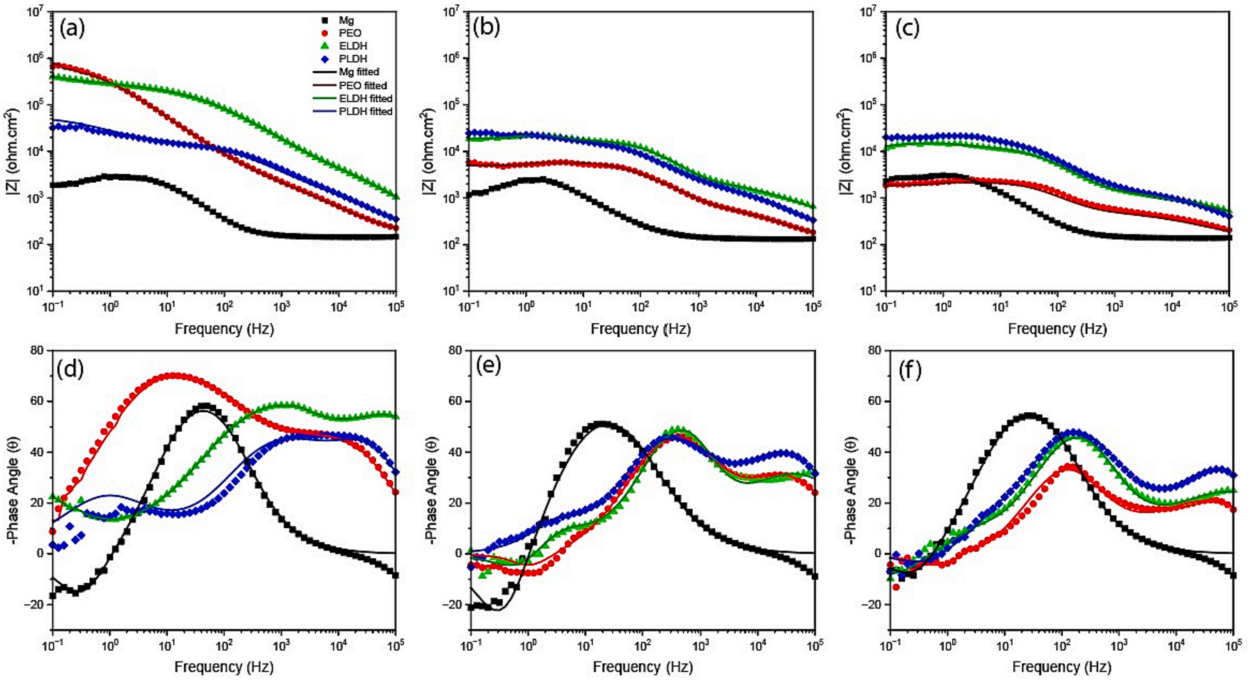

Fig. 5. Impedance spectra obtained for samples after (a), (d) 1 h, (b), (e) 24 h, and (c), (f) 7 days immersion in 0.1 M NaCl solution.

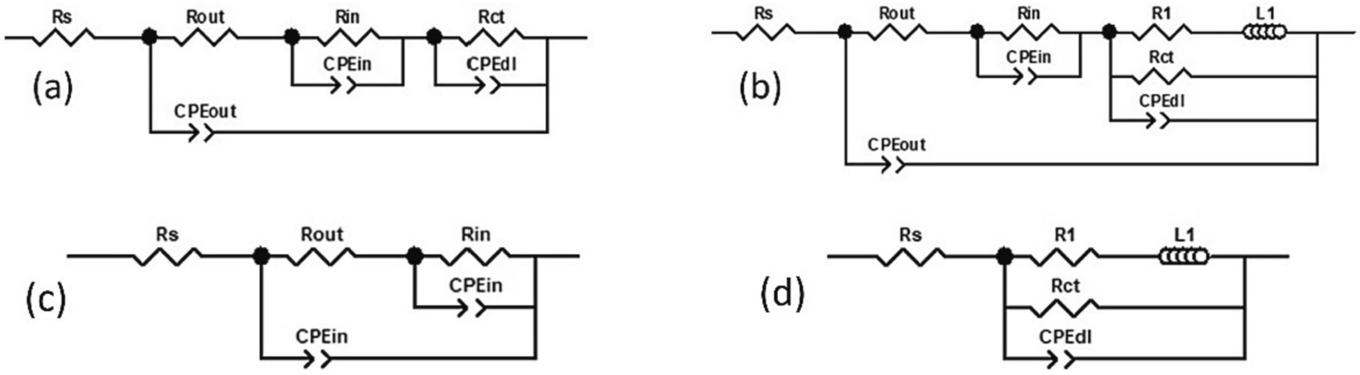

Fig. 6. Equivalent circuits used to fit the EIS data.

Table 1
Results of fitted EIS diagrams for samples at different immersion times.

Sample	R_1 ($\Omega \cdot cm^2$)	L_1 (Henry)	R_{out} ($\Omega \cdot cm^2$)	CPE_{out} ($\Omega^{-1} \cdot s^n \cdot cm^{-2}$)	n	R_{in} ($\Omega \cdot cm^2$)	CPE_{in} ($\Omega^{-1} \cdot s^n \cdot cm^{-2}$)	n	R_{ct} ($\Omega \cdot cm^2$)	CPE_{dl} ($\Omega^{-1} \cdot s^n \cdot cm^{-2}$)	n
Mg-1h	3214	2270	–	–	–	–	–	–	2942	1.1×10^{-5}	0.88
Mg-1d	1516	1181	–	–	–	–	–	–	2770	2.8×10^{-5}	0.80
Mg-7d	6304	4541	–	–	–	–	–	–	3243	2.0×10^{-5}	0.84
PEO-1h	–	–	1343	3.6×10^{-8}	0.96	7.8×10^{5}	6.1×10^{-7}	0.78	–	–	–
PEO-1d	220	120	374	3.6×10^{-8}	0.96	4681	9.7×10^{-7}	0.82	1153	7.3×10^{-5}	0.82
PEO-7d	952	350	168	7.6×10^{-8}	0.89	1065	2.7×10^{-6}	0.99	977	8.2×10^{-5}	0.82
ELDH-1h	–	–	2298	3.0×10^{-9}	0.94	2.9×10^{6}	1.5×10^{-7}	0.64	2.9×10^{6}	1.1×10^{-5}	0.74
ELDH-1d	956	343	2028	7.9×10^{-8}	0.80	15,390	6.8×10^{-8}	0.99	5932	7.9×10^{-5}	0.70
ELDH-7d	235	2696	1042	1.4×10^{-7}	0.80	10,113	2.6×10^{-7}	0.99	4793	8.1×10^{-5}	0.77
PLDH-1h	–	–	1540	4.6×10^{-8}	0.86	13,307	5.9×10^{-7}	0.68	41,615	1.4×10^{-5}	0.69
PLDH-1d	16,297	1207	1224	6.1×10^{-8}	0.84	12,944	6.2×10^{-7}	0.75	37,588	2.1×10^{-5}	0.70
PLDH-7d	9106	1709	900	8.1×10^{-8}	0.79	11,981	7.1×10^{-7}	0.81	26,865	2.5×10^{-5}	0.79

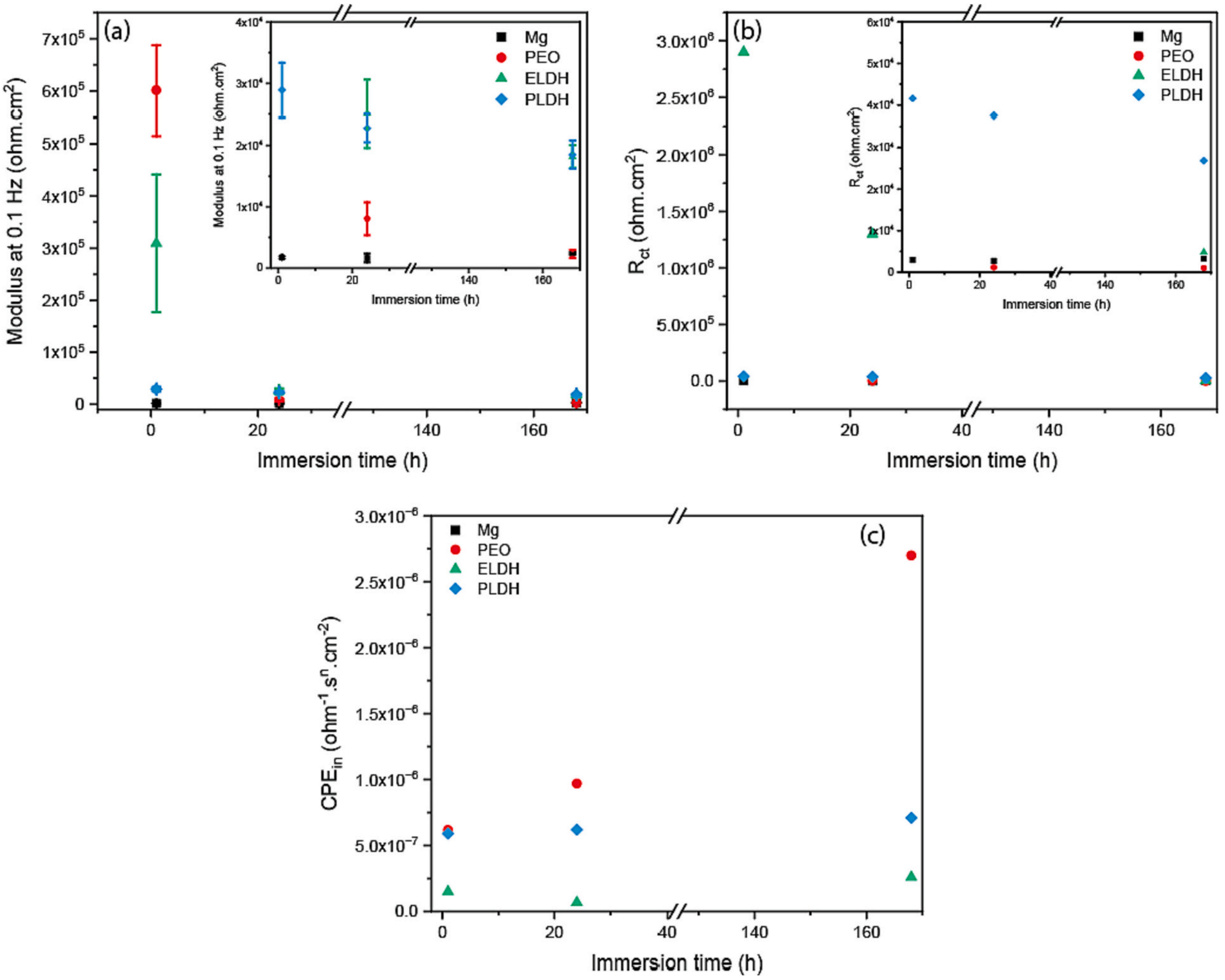

Fig. 7. Evolution of a) impedance modulus at frequency 0.1 Hz, b) R_{ct}, and c) CPE_{in} for all of the samples at different immersion times.

3.3. Evaluation of benzoxazine coatings adhesion

Comparing images of the samples after the cross-cut adhesion test (6 parallel and 6 perpendicular lines) as well as measurements for the surface roughness (Fig. 8(e)) show better compatibility of the benzoxazine with LDH samples. According to Fig. 8(b), the PEO coating does

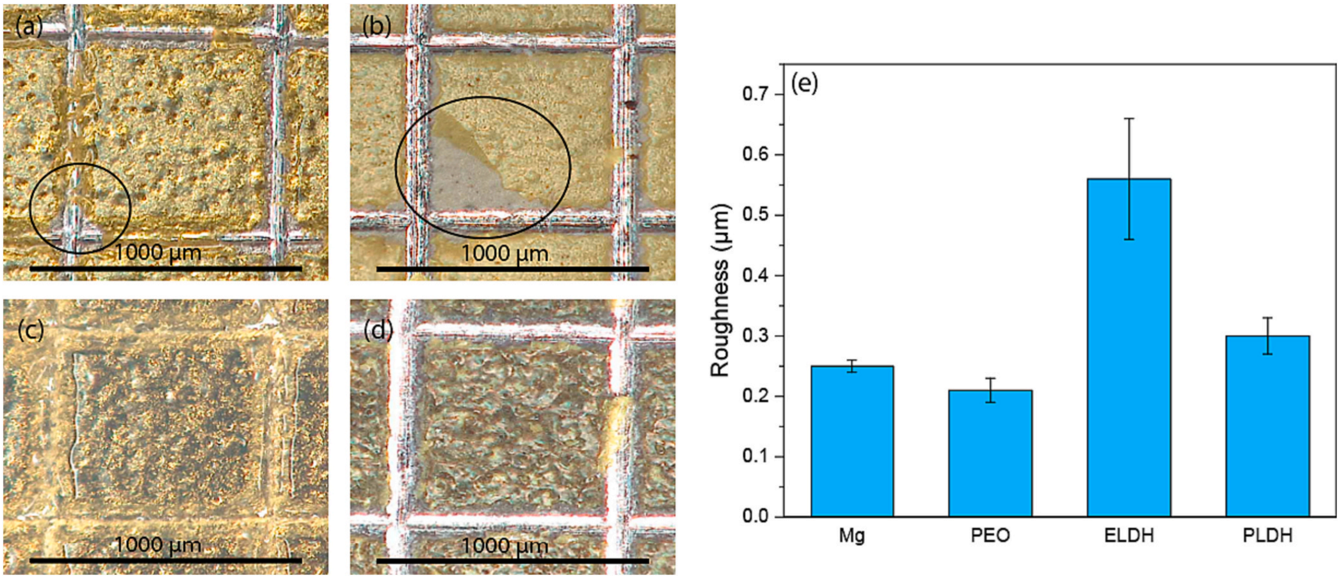

Fig. 8. The cross-cut adhesion test images for a) Mg/B, b) PEO/B, c) ELDH/B, and d) PLDH/B. e) Surface roughness (R_a) of samples covered with benzoxazine resin.

not have proper adhesion to the benzoxazine (the marked part in Fig. 8 (b)). Etching of bare Mg substrate can increase the roughness of the surface which can increase the adhesion of the organic coating. This can be the reason for better adhesion of benzoxazine coating to Mg substrate than the sample with PEO layer. Investigating the interaction energies between benzoxazine and the surfaces of various samples (Mg, PEO, ELDH, and PLDH) will be further discussed (chemical effect investigation).

3.4. Electrochemical measurements (EIS) with benzoxazine resin

The Bode plots of EIS test for samples with benzoxazine coating after immersing samples in 0.1 M NaCl solution for 1 h, 24 h, and 7 days are shown in Fig. 9.

In all of the samples coated with benzoxazine resin, improvement in corrosion resistance is observed while comparing the same samples without benzoxazine resin (Fig. 5). The evolution of impedance (at frequency 0.1 Hz) in Bode diagrams with time shows decrease in corrosion resistance of Mg/benzoxazine (Mg/B) and PEO/benzoxazine (PEO/B). After immersion of PEO/B for 7 days, the sample was corroded intensely which made it unable to measure impedance. However, for the samples with LDH coating, the impedance at low frequency was quite constant with time while it shows higher modulus impedance for ELDH/benzoxazine (ELDH/B) than PLDH/benzoxazine (PLDH/B) (10^7 Ω.cm^2 and 2×10^6 Ω.cm^2 for ELDH/B and PLDH/B after 7 days immersion, respectively). The phase diagram of ELDH/B is almost constant for different immersion times, showing proper protectivity of this coating while for PLDH/B after 1 day of immersion, another time constant at mid-frequency appeared (would be explained further). For fitting the impedance data, the equivalent circuits in Fig. 10 were used.

In these circuits, R_{coat} and CPE_{coat} are related to the resistance and constant phase elements of the benzoxazine coatings. Due to the penetration of electrolyte in benzoxazine coating and formation of the metal-electrolyte interface, another loop is added to the equivalent circuit of samples and shows charge transfer resistance (R_{ct}) and double layer capacitance (CPE_{dl}). The circuit in Fig. 10(a) is used for fitting data of Mg/B samples during the whole immersion times. For this sample, the decrease in R_{coat} (from 7×10^6 to 7960 Ω·cm^2) and R_{ct} (from 339,820 to 1858 Ω·cm^2) after 7 days of immersion can be seen in Table 2, showing the decrease in protectivity of the coating.

For fitting results of PEO/B after 1 h circuit in Fig. 10(b) was used which shows the resistance (R_{PEO}) and constant phase elements (CPE_{PEO}) of the PEO coating, however, after 1 day immersion, another loop is added which corresponds to the inductive peak in the Bode phase diagram of this sample (R_1 and L_1 in Fig. 10(c)). Fig. 10(d) shows the circuit related to ELDH/B for all of the immersion times. In this figure, R_{LDH} and CPE_{LDH} are related to the LDH layer. The decrease in resistance (from 505,570 to 190,660 Ω·cm^2) and increase in constant phase elements (from 3.9×10^{-9} to 4.5×10^{-9} $\Omega^{-1}\cdot s^n\cdot cm^{-2}$) of the coating can be observed in Table 2 showing the loss of coating protection. The fitting of PLDH/B EIS results after 1 h and 24 h immersion was performed using Fig. 10(d). The addition of a time constant in mid-frequency (from 10^0 to 10^2 Hz) in the Bode phase diagram of PLDH/B after 7 days immersion can be attributed to the penetration of electrolyte and creating the loop related to the metal-electrolyte interface (R_{ct} and CPE_{dl} in Fig. 10(e)).

According to the fitting data, the highest R_{coat} value after 7 days immersion is related to the samples with LDH (as the surface pretreatment) and more specifically ELDH/B, representing proper corrosion resistance of the coating that can be attributed to the better adhesion of benzoxazine coatings to LDH layer as well as better corrosion resistance of ELDH (R_{ct} with the value of 2.9×10^6 Ω·cm^2). The value of fitting data is presented in Table 2. CPE as a descriptor of the non-faradic electrochemical process, cannot be defined as a physical parameter, hence, effective capacitance should be calculated according to Eq. (1) to have practical information [36,37].

$$C_{eff} = Y_0^{1/n} \times R_{coat}^{(1-n)/n} \times sin\,(n\pi/2) \quad (1)$$

In this equation, Y_0 and n are the characteristic parameters of CPE. Fig. 11 shows increase in the calculated effective capacitance (C_{eff}) of the organic coatings of all the samples. Increase in the values of C_{eff} is related to the penetration of the electrolyte and higher amount of dielectric constant of water in comparison to the organic coatings [38]

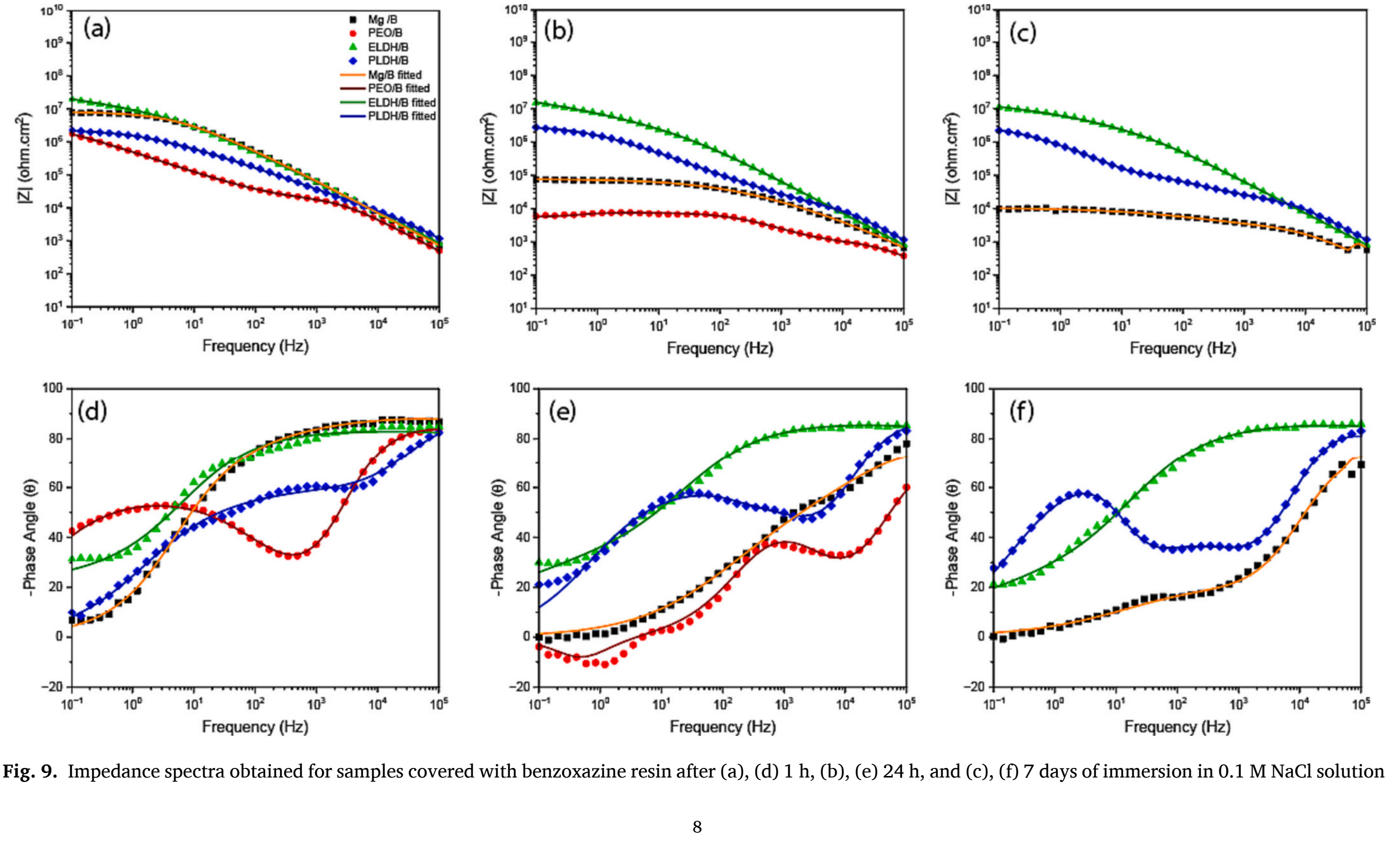

Fig. 9. Impedance spectra obtained for samples covered with benzoxazine resin after (a), (d) 1 h, (b), (e) 24 h, and (c), (f) 7 days of immersion in 0.1 M NaCl solution.

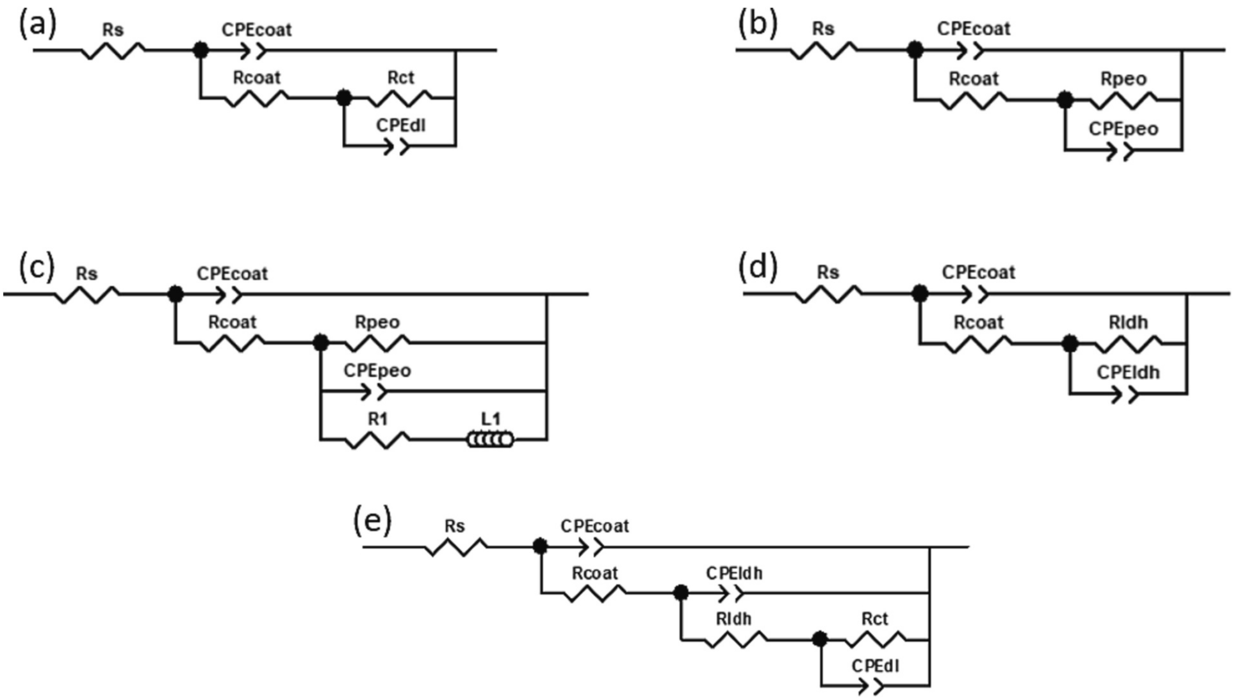

Fig. 10. Equivalent circuits used to fit the EIS data from samples with benzoxazine coating.

Table 2
Results of fitted EIS diagrams for samples with benzoxazine coating at different immersion times.

Sample	R_1 ($\Omega\cdot cm^2$)	L_1 (Henry)	R_{coat} ($\Omega\cdot cm^2$)	CPE_{coat} ($\Omega^{-1}\cdot s^n\cdot cm^{-2}$)	n	R_{PEO}/R_{LDH} ($\Omega\cdot cm^2$)	CPE_{PEO}/CPE_{LDH} ($\Omega^{-1}\cdot s^n\cdot cm^{-2}$)	n	R_{ct} ($\Omega\cdot cm^2$)	CPE_{dl} ($\Omega^{-1}\cdot s^n\cdot cm^{-2}$)	n
Mg/B-1h	–	–	7×10^6	5.5×10^{-9}	0.92	–	–	–	339,820	1.4×10^{-5}	0.90
Mg/B-1d	–	–	65,671	1.3×10^{-7}	0.69	–	–	–	6566	1.5×10^{-5}	0.90
Mg/B-7d	–	–	7960	8.1×10^{-7}	0.70	–	–	–	1858	7.4×10^{-5}	0.89
PEO/B-1h	–	–	18,271	5.1×10^{-9}	0.96	4.9×10^6	5.9×10^{-7}	0.64	–	–	–
PEO/B-1d	15,806	6130	1033	1.5×10^{-8}	0.89	6613	6.1×10^{-7}	0.75	–	–	–
PEO/B-7d	–	–	–	–	–	–	–	–	–	–	–
ELDH/B-1h	–	–	1.06×10^7	5.8×10^{-10}	0.8	3×10^7	8.3×10^{-8}	0.77	–	–	–
ELDH/B-1d	–	–	191,530	4.3×10^{-9}	0.94	2.5×10^7	5.6×10^{-8}	0.50	–	–	–
ELDH/B-7d	–	–	190,660	4.5×10^{-9}	0.93	1.6×10^7	6.1×10^{-8}	0.50	–	–	–
PLDH/B-1h	–	–	6446	1.0×10^{-9}	0.99	2.41×10^6	1.0×10^{-7}	0.61	–	–	–
PLDH/B-1d	–	–	13,447	1.6×10^{-9}	0.98	3.13×10^6	1.2×10^{-7}	0.67	–	–	–
PLDH/B-7d	–	–	13,084	1.5×10^{-9}	0.99	8×10^6	2.4×10^{-7}	0.64	5.2×10^5	6.3×10^{-5}	0.99

as according to Eq. (2) the dielectric constant (ε) is in direct relation with the amount of capacitance (ε_0, A, and d represent the dielectric constant of medium and space, testing area, and distance, respectively [39]):

$$C = \varepsilon\varepsilon_0 A/d \tag{2}$$

It can be observed that the value of C_{eff} is the lowest for samples with LDH which can be attributed to the better adhesion of the organic coating and preventing further penetration of electrolyte for these samples.

3.5. Salt spray

Fig. 12 shows the images of the tested specimen before and after 1 day and 7 days of exposure in the salt spray chamber. The images of samples without benzoxazine show the corrosion occurrence after 1 day which is the least for ELDH. With the application of benzoxazine, the samples could be protected for 1 day except for PEO/B. The benzoxazine coatings on the etched surface of Mg showed some small blisters after 1 day while for the benzoxazine coating on PEO, vivid signs of corrosion could be observed. Moreover, after 7 days, the coatings on these two samples were completely ruined. After 7 days, no visible changes were observed in the coatings applied on the LDH (ELDH and PLDH), indicating the compatibility of the coating with the LDH surface and their effective protective properties.

3.6. DFT calculations

DFT calculations were used to investigate the interaction energy

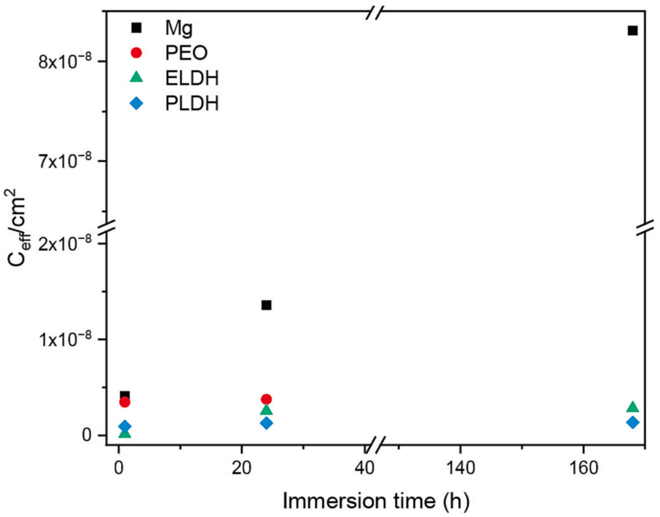

Fig. 11. Effective capacitance (Ceff) of benzoxazine coating calculated from CPEcoat.

between benzoxazine resin and surfaces of Mg, MgO, $Mg(OH)_2$, and $Mg_6Al_2(CO_3)(OH)_{16}$. MgO can be used for simulating the surface of the PEO layer as MgO peaks are mostly observed in XRD diagram of PEO (Fig. 4(b)) and $Mg_6Al_2(CO_3)(OH)_{16}$ for LDH surface. The geometry optimization of the organic molecule/surface interface was done by relaxing the position of the molecule and the top layers of the Mg-based surfaces using the conjugated gradient algorithm until the atomic forces were lower than 0.01 eV/Å.

The interaction energy, E_{int}, was calculated by the difference between the total energy of the relaxed molecule/Mg surface ($E_{mol/Mg}$) and the energy of the molecule (E_{mol}) and surface (E_{surf}) alone, in their relaxed interface geometry.

$$E_{int} = E_{mol/Mg} - \left[E_{Mg} + E_{mol}\right]$$

The atomic charges and bond orders were computed from the DFT electronic density using the DDEC/6 partition scheme [40]. The sum of bond order (SBO) was defined by summing all A_m-A_s atomic pairs where A_m is any atom of the organic molecule and A_s is any atom of the surface. This quantity is used as an indicator of the chemical anchoring of the organic molecule with the surface.

Table 3 is related to the unit cell and electronic properties for the four investigated interfaces in which (a, b) are the surface lattice vectors, and A is the surface occupied by one molecule. The surface thickness was computed as the difference between the atomic positions of the bottom and top atoms of the surface. Q_{mol} is the sum of atomic charges on the adsorbed molecule.

Fig. 13 shows the schematic illustration of structures and their charge transfer. The pristine Mg surface shows that the molecule used as an organic coating has a strong interaction with magnesium (an interacting energy of −2.62 eV). The SBO is also large and equivalent to 3 single covalent bonds. A deeper analysis of the BO pair shows that the interaction is mainly driven by three connections between the molecule and the surface: 2 O—Mg bonds (bond length of 2.12 Å and 2.27 Å with BO of 0.44 and 0.55) and 1 N-Mg bond (bond length of 2.29 Å and BO of 0.40). The intensity of these connections leads to a displacement of the Mg atoms from the surface plane to the molecule by 0.25–0.57 Å. A similar interaction energy is obtained for the MgO surface (−2.65 eV) while the charge transfer from the surface to the molecule is reduced compared to Mg (−0.082|e| vs −0.245 |e|). By comparison, the pristine magnesium hydroxide surface $Mg(OH)_2$ exhibits a lower interaction energy of −1.51 eV. The charge transfer is also inverted with electrons moving from the molecule into the surface. The presence of aluminum in the structure and carbonate between layers has a large impact on the result. The first effect is the displacement between the two (HO-metal-OH) layers. In the case of pristine $Mg(OH)_2$ the distance between the two metal layers is 4.58 Å. This distance increases to reach 6.23 Å for our

Table 3
Unit cell and electronic properties for the four investigated interfaces.

	Mg	MgO	$Mg(OH)_2$	$Mg_6Al_2(CO_3)(OH)_{16}$
(a,b) (Å)	19.06 × 15.88	16.98 × 12.74	12.70 × 15.87	12.70 × 15.87
A (Å^2)	262.2	216.3	174.53	174.53
Thickness (Å)	7.8	6.3	8.6	10.7
E_{int} (eV)	−2.62	−2.65	−1.51	−3.60
Q_{mol} (e)	−0.245	−0.082	+0.118	−0.053
SBO	3.04	2.14	1.56	2.25

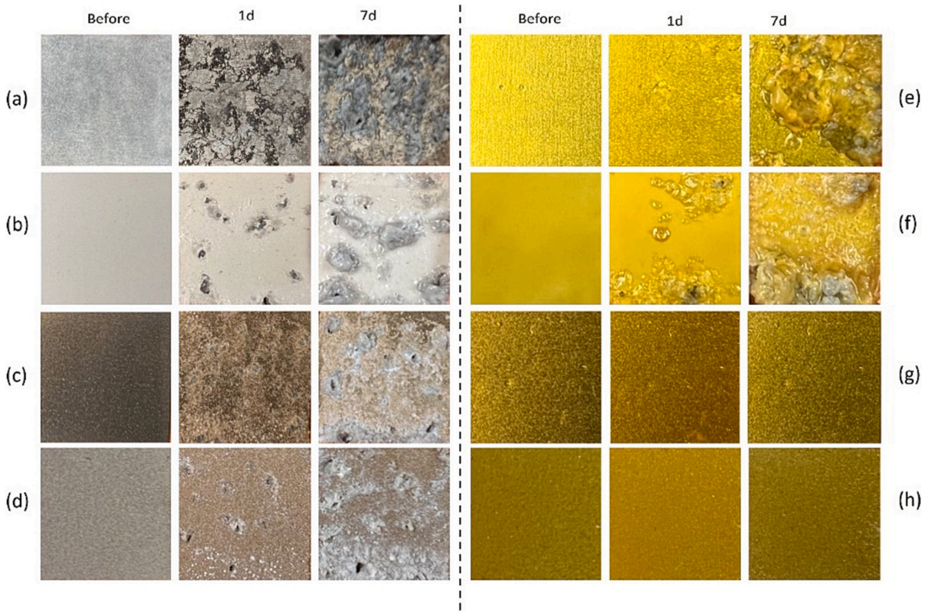

Fig. 12. Macroscopic images of the samples before and after salt spray test a) Mg, b) PEO, c) ELDH, d) PLDH, e) Mg/B, f) PEO/B, g) ELDH/B, and h) PLDH/B.

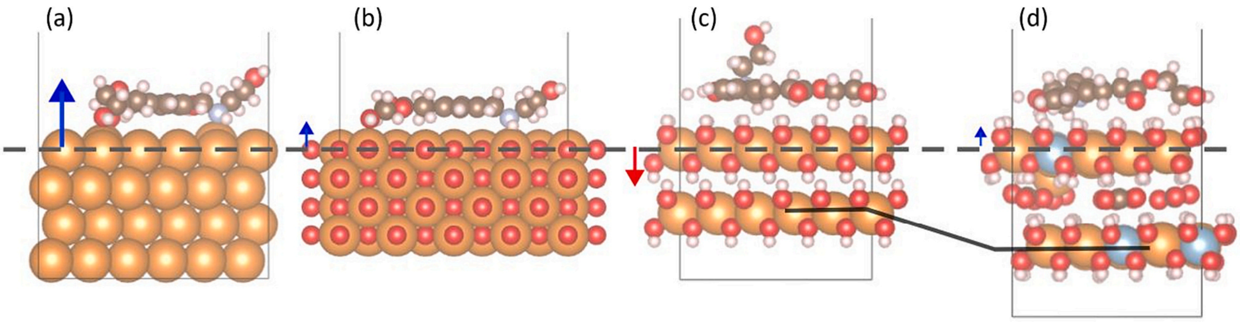

Fig. 13. Side views of computational models for the optimized adsorbed structure of simplified benzoxazine molecule onto the (a) Mg, (b) MgO, (c) $Mg(OH)_2$, and (d) $Mg_6Al_2(CO_3)(OH)_{16}$ surface. The orange, red, brown, white, small, and big blue balls stand for Mg, O, C, H, N, and Al atoms, respectively. The size and direction of arrows represent the intensity of the charge transfer. The dashed line is the surface, and all structures are shifted to have the surface at the same position. The increase of the $Mg_6Al_2(CO_3)(OH)_{16}$ layers is shown by the full line. (For interpretation of the references to colour in this figure legend, the reader is referred to the web version of this article.)

model i.e. $Mg_6Al_2(CO_3)(OH)_{16}$. Mg to Al substitution leads also to a weak charge transfer (due to the presence of the carbonate which balanced the charges at the interface) that is 0.053 |e| moving from the metal into the molecule while for $Mg(OH)_2$ it is 0.118 |e| going in the opposite way. The presence of aluminum atoms increases the interaction energy which reaches −3.6 eV i.e. a value comparable to those obtained on the pristine Mg and MgO surfaces. In the case of carbonate, a third contribution can be present implying electrostatic pair interaction (i.e. a coulombic interaction between each point charge). This contribution should be higher in $Mg_6Al_2(CO_3)(OH)_{16}$ due to the large charge dispersity while for pure Mg, the metal layers have globally a small net charge. To summarize, in the DFT calculations for investigating the interactions in detail, the proper compatibility of the benzoxazine molecule with Mg was detected and it was observed that the existence of Al as well as carbonate in the interlayer can increase the interaction energy with the organic molecule.

These results are in good agreement with the results obtained from adhesion tests. Moreover, the effect of the adhesion of organic coatings to the substrate on the corrosion resistance of the substrate is more than the diffusion of corrosive ions to the substrate [15]. Thus, better adhesion of the coating can increase the corrosion resistance. In the case of Mg and MgO as the surfaces of etched Mg substrate and PEO layer, the interaction energy is almost the same while the charge transfer is more for organic molecule and Mg surface (in comparison to organic molecule and MgO surface). These results are in accordance with the better corrosion resistance of Mg/B than PEO/B (Figs. 9(a), (b) and 12(e), (f)). $Mg_6Al_2(CO_3)(OH)_{16}$ structure, which can be a model for LDH layer, is crucial to have better interaction energy and consequently better adhesion of the surface to the organic coating. According to DFT results and better adhesion of the benzoxazine molecule to the LDH model, the corrosion resistance should be improved which is in agreement with the experimental results of EIS and salt spray tests. Therefore, even though surface pretreatments (etching and PEO) can increase corrosion resistance, the formation of LDH is necessary in the case of post-treatment with organic coatings to improve their adhesion and consequently the corrosion resistance.

4. Conclusion

In this study, LDH was successfully formed on the surface of the etched and PEO layer of AZ31 Mg alloy via one-step hydrothermal treatment. The proper corrosion resistance of LDH produced on the etched substrate was observed during 7 days of immersion in 0.1 M NaCl solution. This sample showed better corrosion resistance due to the thicker LDH inner layer in comparison to the LDH on PEO layer. Moreover, the samples were post-treated with a new bio-based benzoxazine resin for further sealing and corrosion enhancement of samples. The produced benzoxazine resin showed proper compatibility with Mg surfaces and increased corrosion resistance. However, the best corrosion resistance was observed for LDH samples with benzoxazine resin attributing to the appropriate adhesion of benzoxazine to the LDH layer. These results were confirmed by cross-cut adhesion test and DFT calculations. Therefore, it was shown that the existence of LDH along with our organic coating can physically and chemically enhance the corrosion resistance of magnesium alloys.

CRediT authorship contribution statement

Roya Malekkhouyan: Writing – original draft, Methodology, Investigation, Formal analysis, Conceptualization. **Louis Van Renterghem:** Validation, Investigation, Formal analysis. **Leila Bonnaud:** Validation, Supervision, Methodology, Data curation. **Yoan Paint:** Validation, Investigation. **Maurice Gonon:** Validation, Investigation. **David Cornil:** Validation, Software, Methodology, Investigation. **Jérôme Cornil:** Validation, Supervision, Methodology. **Jean-Marie Raquez:** Writing – review & editing, Validation, Supervision, Project administration, Methodology. **Marie-Georges Olivier:** Writing – review & editing, Validation, Supervision, Methodology, Funding acquisition, Conceptualization.

Declaration of competing interest

The authors declare that they have no known competing financial interests or personal relationships that could have appeared to influence the work reported in this paper.

Data availability

Data will be made available on request.

Acknowledgments

This research was funded by La Fédération Wallonie-Bruxelles (Belgium) through University of MONS (UMONS), ARC 2020 (Actions de Recherche Concertées) - PROCOMAG project, Grants attributed to Roya Malekkhouyan and Louis Van Renterghem.

References

[1] M. Toorani, M. Aliofkhazraei, Review of electrochemical properties of hybrid coating systems on mg with plasma electrolytic oxidation process as pretreatment, Surf. Interfaces 14 (2019) 262–295, https://doi.org/10.1016/j.surfin.2019.01.004.
[2] G.L. Song, A. Atrens, Corrosion mechanisms of magnesium alloys, Adv. Eng. Mater. 1 (1) (1999) 11–33, https://doi.org/10.1002/(SICI)1527-2648(199909)1:1<11::AID-ADEM11>3.0.CO;2-N.

[3] C. Zhao, X. Wang, B. Yu, M. Cai, Q. Yu, F. Zhou, Research progress on the wear and corrosion resistant plasma electrolytic oxidation composite coatings on magnesium and its alloys, Coatings 13 (7) (2023), https://doi.org/10.3390/coatings13071189.

[4] R.O. Hussein, D.O. Northwood, X. Nie, The effect of processing parameters and substrate composition on the corrosion resistance of plasma electrolytic oxidation (PEO) coated magnesium alloys, Surf. Coat. Technol. 237 (2013) 357–368, https://doi.org/10.1016/j.surfcoat.2013.09.021.

[5] R. Hussein, D. Northwood, X. Nie, The influence of pulse timing and current mode on the microstructure and corrosion behaviour of a plasma electrolytic oxidation (PEO) coated AM60B magnesium alloy, J. Alloys Compd. 541 (2012) 41–48, https://doi.org/10.1016/j.jallcom.2012.07.003.

[6] H. Li, S. Lu, W. Qin, L. Han, X. Wu, Improving the wear properties of AZ31 magnesium alloy under vacuum low-temperature condition by plasma electrolytic oxidation coating, Acta Astronaut. 116 (2015) 126–131, https://doi.org/10.1016/j.actaastro.2015.07.005.

[7] F. Muhaffel, H. Cimenoglu, Development of corrosion and wear resistant micro-arc oxidation coating on a magnesium alloy, Surf. Coat. Technol. 357 (2019) 822–832, https://doi.org/10.1016/j.surfcoat.2018.10.089.

[8] W. Yao, L. Wu, J. Wang, B. Jiang, D. Zhang, M. Serdechnova, T. Shulha, C. Blawert, M.L. Zheludkevich, F. Pan, Micro-arc oxidation of magnesium alloys: a review, J. Mater. Sci. Technol. 118 (2022) 158–180, https://doi.org/10.1016/j.jmst.2021.11.053.

[9] A. Fattah-alhosseini, M. Sabaghi Joni, Effect of KOH concentration on the microstructure and electrochemical properties of MAO-coated Mg alloy AZ31B, J. Mater. Eng. Perform. 24 (9) (2015) 3444–3452, https://doi.org/10.1007/s11665-015-1645-4.

[10] G. Mishra, B. Dash, S. Pandey, Layered double hydroxides: a brief review from fundamentals to application as evolving biomaterials, Appl. Clay Sci. 153 (2018) 172–186, https://doi.org/10.1016/j.clay.2017.12.021.

[11] Y. Chen, L. Wu, W. Yao, Z. Zhong, Y. Chen, J. Wu, F. Pan, One-step in situ synthesis of graphene oxide/MgAl-layered double hydroxide coating on a micro-arc oxidation coating for enhanced corrosion protection of magnesium alloys, Surf. Coat. Technol. 413 (2021) 127083, https://doi.org/10.1016/j.surfcoat.2021.127083.

[12] Y. Chen, L. Wu, W. Yao, Y. Chen, Z. Zhong, W. Ci, J. Wu, Z. Xie, Y. Yuan, F. Pan, A self-healing corrosion protection coating with graphene oxide carrying 8-hydroxyquinoline doped in layered double hydroxide on a micro-arc oxidation coating, Corros. Sci. 194 (2022) 109941, https://doi.org/10.1016/j.corsci.2021.109941.

[13] G.-L. Song, "Electroless" deposition of a pre-film of electrophoresis coating and its corrosion resistance on a Mg alloy, Electrochim. Acta 55 (7) (2010) 2258–2268, https://doi.org/10.1016/j.electacta.2009.11.078.

[14] R.-G. Hu, S. Zhang, J.-F. Bu, C.-J. Lin, G.-L. Song, Recent progress in corrosion protection of magnesium alloys by organic coatings, Prog. Org. Coat. 73 (2–3) (2012) 129–141, https://doi.org/10.1016/j.porgcoat.2011.10.011.

[15] Grundmeier, G., Schmidt, W., and Stratmann, M., Electrochim Acta 45: 2515 doi: 10.1016. S0013-4686 (00), 2000: p. 00348-0.

[16] C. Zhang, X. Luo, R. Zhu, H. Ling, Y. Gu, Thermal and dielectric properties of epoxy/DDS/CTBN adhesive modified by cardanol-based benzoxazine, J. Adhes. Sci. Technol. 29 (8) (2015) 767–777, https://doi.org/10.1080/01694243.2015.1004508.

[17] Y. Yagci, B. Kiskan, N.N. Ghosh, Recent advancement on polybenzoxazine—a newly developed high performance thermoset, J. Polym. Sci. A Polym. Chem. 47 (21) (2009) 5565–5576, https://doi.org/10.1002/pola.23597.

[18] A. Renaud, M. Poorteman, J. Escobar, L. Dumas, Y. Paint, L. Bonnaud, P. Dubois, M.-G. Olivier, A new corrosion protection approach for aeronautical applications combining a Phenol-paraPhenyleneDiAmine benzoxazine resin applied on sulfo-tartaric anodized aluminum, Prog. Org. Coat. 112 (2017) 278–287, https://doi.org/10.1016/j.porgcoat.2017.07.007.

[19] F.W. Holly, A.C. Cope, Condensation products of aldehydes and ketones with o-aminobenzyl alcohol and o-hydroxybenzylamine, J. Am. Chem. Soc. 66 (11) (1944) 1875–1879, https://doi.org/10.1021/ja01239a022.

[20] M.W. Wang, R.J. Jeng, C.H. Lin, Study on the ring-opening polymerization of benzoxazine through multisubstituted polybenzoxazine precursors, Macromolecules 48 (3) (2015) 530–535, https://doi.org/10.1021/ma502336j.

[21] H. Li, J. Gu, D. Wang, C. Qu, Y. Zhang, Study on benzoxazine-based film adhesive and its adhesion properties with CFPR composites, J. Adhes. Sci. Technol. 31 (16) (2017) 1796–1806, https://doi.org/10.1080/01694243.2017.1283889.

[22] V. Kasneryk, M. Serdechnova, C. Blawert, M.L. Zheludkevich, LDH has been grown: what is next? Overview on methods of post-treatment of LDH conversion coatings, Appl. Clay Sci. (2023) 232, https://doi.org/10.1016/j.clay.2022.106774.

[23] L. Wu, D. Yang, G. Zhang, Z. Zhang, S. Zhang, A. Tang, F. Pan, Fabrication and characterization of Mg-M layered double hydroxide films on anodized magnesium alloy AZ31, Appl. Surf. Sci. 431 (2018) 177–186, https://doi.org/10.1016/j.apsusc.2017.06.244.

[24] G. Kresse, D. Joubert, From ultrasoft pseudopotentials to the projector augmented-wave method, Phys. Rev. B 59 (3) (1999) 1758, https://doi.org/10.1103/PhysRevB.59.1758.

[25] G. Kresse, J. Furthmüller, Efficient iterative schemes for ab initio total-energy calculations using a plane-wave basis set, Phys. Rev. B 54 (16) (1996) 11169, https://doi.org/10.1103/PhysRevB.54.11169.

[26] J.P. Perdew, K. Burke, M. Ernzerhof, Generalized gradient approximation made simple, Phys. Rev. Lett. 77 (18) (1996) 3865, https://doi.org/10.1103/PhysRevLett.77.3865.

[27] S. Grimme, J. Antony, S. Ehrlich, H. Krieg, A consistent and accurate ab initio parametrization of density functional dispersion correction (DFT-D) for the 94 elements H-Pu, J. Chem. Phys. 132 (15) (2010), https://doi.org/10.1063/1.3382344.

[28] S. Grimme, S. Ehrlich, L. Goerigk, Effect of the damping function in dispersion corrected density functional theory, J. Comput. Chem. 32 (7) (2011) 1456–1465, https://doi.org/10.1002/jcc.21759.

[29] G. Zhang, L. Wu, A. Tang, Y. Ma, G.-L. Song, D. Zheng, B. Jiang, A. Atrens, F. Pan, Active corrosion protection by a smart coating based on a MgAl-layered double hydroxide on a cerium-modified plasma electrolytic oxidation coating on Mg alloy AZ31, Corros. Sci. 139 (2018) 370–382, https://doi.org/10.1016/j.corsci.2018.05.010.

[30] D. Zhang, J. Zhou, F. Peng, J. Tan, X. Zhang, S. Qian, Y. Qiao, Y. Zhang, X. Liu, Mg-Fe LDH sealed PEO coating on magnesium for biodegradation control, antibacteria and osteogenesis, J. Mater. Sci. Technol. 105 (2022) 57–67, https://doi.org/10.1016/j.jmst.2021.05.088.

[31] R. Malekkhouyan, Y. Paint, L. Prince, M. Gonon, M.-G. Olivier, Controlling lateral size and thickness of layered double hydroxide (LDH) used as conversion layer for corrosion protection of AZ31 Mg alloy, Corros. Mater. Degrad. 4 (1) (2023) 174–195, https://doi.org/10.3390/cmd4010011.

[32] L. Wu, F. Pan, Y. Liu, G. Zhang, A. Tang, A. Atrens, Influence of pH on the growth behaviour of Mg–Al LDH films, Surf. Eng. 34 (9) (2018) 674–681, https://doi.org/10.1080/02670844.2017.1382062.

[33] S. Wang, C. Liu, M. Wang, Y. Chuang, P. Chiang, Arsenate adsorption by Mg/Al–NO3 layered double hydroxides with varying the Mg/Al ratio, Appl. Clay Sci. 43 (1) (2009) 79–85, https://doi.org/10.1016/j.clay.2008.07.005.

[34] L. Wang, D. Snihirova, M.D. Havigh, M. Deng, S.V. Lamaka, H. Terryn, M. L. Zheludkevich, Non-stationarity in electrochemical impedance measurement of Mg-based materials in aqueous media, Electrochim. Acta 468 (2023) 143140, https://doi.org/10.1016/j.electacta.2023.143140.

[35] V.Z. Asl, S.F. Chini, J. Zhao, Y. Palizdar, M. Shaker, A. Sadeghi, Corrosion properties and surface free energy of the ZnAl LDH/rGO coating on MAO pretreated AZ31 magnesium alloy, Surf. Coat. Technol. 426 (2021) 127764, https://doi.org/10.1016/j.surfcoat.2021.127764.

[36] B.-Y. Chang, Conversion of a constant phase element to an equivalent capacitor, J. Electrochem. Sci. Technol. 11 (3) (2020) 318–321, https://doi.org/10.33961/jecst.2020.00815.

[37] B. Hirschorn, M.E. Orazem, B. Tribollet, V. Vivier, I. Frateur, M. Musiani, Determination of effective capacitance and film thickness from constant-phase-element parameters, Electrochim. Acta 55 (21) (2010) 6218–6227, https://doi.org/10.1016/j.electacta.2009.10.065.

[38] I.C.P. Margarit-Mattos, EIS and organic coatings performance: revisiting some key points, Electrochim. Acta (2020) 354, https://doi.org/10.1016/j.electacta.2020.136725.

[39] F. Deflorian, L. Fedrizzi, S. Rossi, P. Bonora, Organic coating capacitance measurement by EIS: ideal and actual trends, Electrochim. Acta 44 (24) (1999) 4243–4249, https://doi.org/10.1016/S0013-4686(99)00139-5.

[40] T.A. Manz, N.G. Limas, Introducing DDEC6 atomic population analysis: part 1. Charge partitioning theory and methodology, RSC Adv. 6 (53) (2016) 47771–47801, https://doi.org/10.1039/C6RA04656H.